Original Article

# Imaging evaluation focused on microstructural tissue changes using tensor-valued diffusion encoding in breast cancers after neoadjuvant chemotherapy: is it a promising way forward?

**Eun Cho[1]^, Hye Jin Baek[1,2]^, Filip Szczepankiewicz[3]^, Hyo Jung An[4]^, Eun Jung Jung[5]^**

[1]Department of Radiology, Gyeongsang National University School of Medicine and Gyeongsang National University Changwon Hospital, Changwon, Republic of Korea; [2]FRIENDS Imaging Center, Busan, Republic of Korea; [3]Department of Diagnostic Radiology, Clinical Sciences Lund, Lund University, Lund, Sweden; [4]Department of Pathology, Gyeongsang National University School of Medicine and Gyeongsang National University Changwon Hospital, Changwon, Republic of Korea; [5]Department of Surgery, Gyeongsang National University School of Medicine and Gyeongsang National University Changwon Hospital, Changwon, Republic of Korea

*Contributions:* (I) Conception and design: E Cho, HJ Baek; (II) Administrative support: HJ Baek, F Szczepankiewicz; (III) Provision of study materials or patients: EJ Jung; (IV) Collection and assembly of data: E Cho, EJ Jung; (V) Data analysis and interpretation: E Cho, HJ Baek, F Szczepankiewicz, HJ An; (VI) Manuscript writing: All authors; (VII) Final approval of manuscript: All authors.

*Correspondence to:* Hye Jin Baek, MD, PhD. Department of Radiology, Gyeongsang National University School of Medicine and Gyeongsang National University Changwon Hospital, 11, Samjeongja-ro, Seongsan-gu, Changwon 51472, Republic of Korea; FRIENDS Imaging Center, 1303, C Building, 123, Centum Dong-ro, Haeundae-gu, Busan, Republic of Korea. Email: sartre81@gmail.com.

**Background:** Single diffusion encoding is a widely used, noninvasive technique for probing the tissue microstructure in breast tumors. However, it does not provide detailed information about the microenvironmental complexity. This study investigated the clinical utility of tensor-valued diffusion encoding for evaluating microstructural changes in breast cancer after neoadjuvant chemotherapy (NAC).

**Methods:** We retrospectively included patients underwent chemotherapy for histologically proven invasive breast cancer between July 2020 and June 2023 and monitored the tumor response with breast magnetic resonance imaging (MRI), including tensor-valued diffusion encoding. We reviewed pre- and post-NAC MRIs regarding chemotherapy in 23 breast cancers. Q-space trajectory imaging (QTI) parameters were estimated at each time-point, and were compared with histopathological parameters.

**Results:** The mean total mean kurtosis ($MK_T$), anisotropic mean kurtosis ($MK_A$), and microscopic fractional anisotropy (μFA) were significantly decreased on post-NAC MRI compared with pre-NAC MRI, with the large effect size (ES) in $MK_A$ and μFA (0.81±0.41 *vs.* 0.99±0.33, ES: 0.48, P=0.03; 0.48±0.30 *vs.* 0.73±0.27, ES: 0.88, P<0.001; 0.58±0.14 *vs.* 0.68±0.11, ES: 0.79, P=0.003; respectively). Regarding prognostic factors, tumors with high Ki-67 expression showed significantly lower pre-NAC mean diffusivity (MD) and higher pre-NAC μFA compared to tumors with low Ki-67 expression (0.98±0.09 *vs.* 1.25±0.20, P=0.002; and 0.72±0.07 *vs.* 0.57±0.10, P=0.005; respectively). And negative progesterone receptor (PR) group revealed significantly lower $MK_T$, $MK_A$, and isotropic mean kurtosis than positive PR group on the post-NAC MRI (0.60±0.31 *vs.* 1.03±0.40, P=0.008; 0.36±0.21 *vs.* 0.61±0.33, P=0.04; and 0.23±0.17 *vs.* 0.42±0.25, P=0.046; respectively).

**Conclusions:** QTI parameters reflected the microstructural changes in breast cancer treated with NAC and can be used as noninvasive imaging biomarkers correlated with prognostic factors.

**Keywords:** Magnetic resonance imaging (MRI); diffusion-weighted imaging (DWI); tensor-valued diffusion encoding; breast cancer; chemotherapy response

^ ORCID: Eun Cho, 0000-0001-7814-7430; Hye Jin Baek, 0000-0001-7349-2841; Filip Szczepankiewicz, 0000-0002-5251-587X; Hyo Jung An, 0000-0002-2068-8370; Eun Jung Jung, 0000-0001-8413-613X.

Submitted Apr 16, 2024. Accepted for publication Aug 05, 2024. Published online Aug 22, 2024.
doi: 10.21037/gs-24-124
**View this article at:** https://dx.doi.org/10.21037/gs-24-124

## Introduction

Neoadjuvant chemotherapy (NAC) is a standard treatment for locally advanced breast cancer (1,2). NAC enables breast conservation, avoids axillary dissection, and renders inoperable cancers operable by tumor downstaging. In addition, it allows the *in vivo* monitoring of tumor response during treatment. Dynamic contrast-enhanced magnetic resonance imaging (DCE-MRI) is the most accurate imaging modality for evaluating tumor response to NAC owing to its high resolution and sensitivity for detecting breast lesions (3,4).

However, there is an ongoing discussion regarding MRI techniques that do not require contrast agents in everyday clinical practice because of the possible side effects and brain deposition of gadolinium contrast media. Therefore, diffusion-weighted imaging (DWI) is emerging as a key imaging technique for detecting and characterizing breast lesions (5,6). DWI is a method of signal contrast generation based on the differences in the Brownian motion of water molecules in biological tissues (7). Based on the diffusion of water molecules through tumoral tissue, DWI is in the spotlight as a useful noninvasive alternative to DCE-MRI for predicting the tumor response to NAC by reflecting microstructural and functional changes (8,9). Conventional DWI using a single diffusion encoding provides apparent diffusion coefficient (ADC) values that reflect tumor cellularity and broad-brush estimates of tissue microstructures (5,6,10). However, previous studies on the association between ADC and post-NAC tumor response show inconsistent results with large variability (8,9,11,12). The previous studies showed that change in ADC values could not reflect changes in the volume of tumor response to chemotherapy (8,9,11). Also, ADC values has a limitation for differentiating the densely fibrotic or sclerotic tissue changes, high cell density, or presence of inflammation in lesions to residual cancer (13-15). Therefore, there has been an increasing effort to apply the models of diffusion tensor invariants based on DWI, such as diffusion tensor imaging (DTI) and diffusion kurtosis imaging (DKI), for evaluating the response to chemotherapy based on the microstructural change in breast cancers (16-18). DTI can provide efficient distinct diffusion parameter such as, fractional anisotropy (FA) which is the most commonly used quantitative anisotropy index. However, some previous studies found that the FA was not significantly changed after underwent chemotherapy or did not help with distinguishing malignancy from benign or fibroglandular tissue (18-21). In addition, the interpretation of DKI parameters in relation to features of tissue microstructure remains unclear (22,23).

Recently, tensor-valued diffusion encoding using multiple directions per signal acquisition has been developed for evaluating the microstructure in multiple organs, including the breast (24-32). The data obtained by the tensor-value diffusion encoding is analyzed using Q-space trajectory imaging (QTI) to decompose the total diffusional variance into two components: 'microscopic anisotropy' related to eccentric cells and tissue structures, and 'isotropic heterogeneity' reflecting variable cell density or tissue mixtures (25,26,33-35). QTI provides five parameters, including mean diffusivity (MD), anisotropic and isotropic mean kurtosis ($MK_A$ and $MK_I$), total mean kurtosis ($MK_T = MK_A + MK_I$), FA, and microscopic fractional anisotropy (μFA). Among the QTI parameters, μFA is considered as a reliable biomarker for evaluating tumors because it is not influenced by the effects of orientation dispersion (31,35).

To the best of our knowledge, only two recent studies have reported that QTI parameters derived from tensor-valued diffusion encoding can help distinguish between

### Highlight box

**Key findings**

- Total mean kurtosis, anisotropic mean kurtosis, and microscopic fractional anisotropy (μFA) showed significant changes after neoadjuvant chemotherapy.
- Mean diffusivity and μFA were correlated with Ki-67 index and progesterone receptor status.

**What is known and what is new?**

- Tensor-valued diffusion encoding provides microstructural information by analyzing with Q-space trajectory imaging (QTI).
- Tensor-valued diffusion encoding reflects microstructural tissue change in breast cancer undergone chemotherapy.

**What is the implication, and what should change now?**

- QTI parameters can be used as noninvasive imaging biomarkers for assessing response to neoadjuvant chemotherapy.

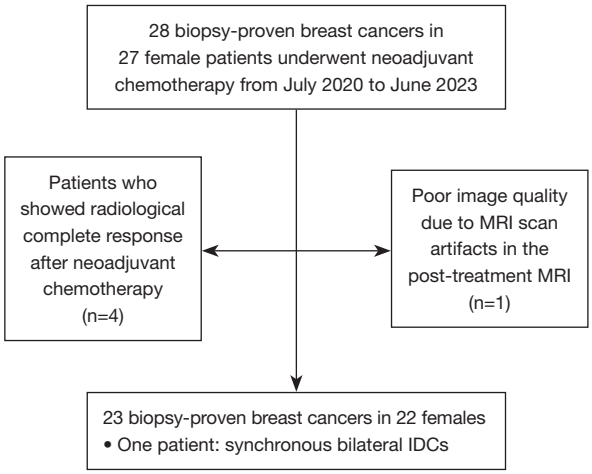


**Figure 1** Flow chart for inclusion of patients. MRI, magnetic resonance imaging; IDC, invasive ductal carcinoma.

fibroglandular breast tissue and breast cancer, reflecting microstructural details (29,31). This study aimed to investigate the clinical utility of tensor-valued diffusion encoding for evaluating microstructural changes in breast cancers by comparing QTI parameters derived from the pre- and post-NAC breast MRI examinations. We present this article in accordance with the STROBE reporting checklist (available at https://gs.amegroups.com/article/view/10.21037/gs-24-124/rc).

## Methods

### *Study population*

This study was conducted according to the Declaration of Helsinki (as revised in 2013). This study was a retrospective analysis of prospectively acquired data. The Institutional Review Board of Gyeongsang National University Changwon Hospital approved this study (IRB No. GNUCH 2023-03-043), and the requirement for individual consent was waived in view of the retrospective nature of the study. Patient records and information were anonymized and de-identified prior to the analysis.

We searched the picture archiving and communication system reports and electronic medical records of patients with breast cancers who underwent NAC and pre- and post-NAC MRI between from July 2020 and June 2023. We identified 27 female patients with 28 breast cancers. We excluded four patients with radiologically complete remission on post-NAC MRI because no overt lesions were noted on the images. We also excluded one patient with insufficient diagnostic image quality due to magnetic susceptibility artifacts induced by the chemoport on the post-NAC MRI. Finally, we enrolled 22 patients with 23 breast cancers (mean age, 51.5±9.5 years; range, 38–71 years); one patient had synchronous bilateral breast cancers (*Figure 1*). Seventeen patients (18 of 23 cancers) underwent breast cancer surgery at our institution whereas the other three patients with distant metastases at the time of diagnosis did not undergo surgical removal of the index cancer. In addition, we reviewed the clinical prognostic cancer stages at the time of diagnosis and the pathological prognostic cancer stages after NAC, according to the 8$^{th}$ edition of the American Joint Committee on Cancer (AJCC) (36).

### *MRI examination protocol*

MRI was performed using a 3T system (Signa$^{TM}$ Architect, GE Healthcare, Waukesha, Wisconsin, USA) with an 8-channel breast coil in the prone position supplemented with a prototype tensor-valued diffusion encoding sequence. The breast MRI protocol included: (I) three-dimensional (3D) Dixon-based fat-suppressed T2-weighted sequence [repetition time (TR) =2,000 ms, echo time (TE) =90 ms, in-plane resolution =0.7×0.7 mm$^2$, acquisition time =3 min]; (II) DCE high temporal and spatial resolution 3D T1-weighted sequence with dual-echo 3D spoiled gradient echo sequence with Dixon fat-water separation (TR =5.0 ms, TE =1.7 ms, flip angle =10 degrees, in-plane resolution =0.7×0.7 mm$^2$, acquisition time =8 min); (III) echo-planar imaging based conventional DWI using a single diffusion encoding with *b*-values 0 and 800 s/mm$^2$ (TR =2,970 ms, TE =82 ms, number of excitations =6, in-plane resolution =1.3×1.3 mm$^2$, slice thickness =5.0 mm, slice number =38, acquisition time =3 min 27 s). Tensor-valued diffusion encoding was performed using a vendor-provided pulse sequence prototype. We used both linear and spherical *b*-tensor encoding at three *b*-values of 100, 1,000, and 2,000 s/mm$^2$, where the linear *b*-tensor encoding was directed along the [4 10 15] direction, and the spherical *b*-tensor encoding was repeated [6 10 10] times for each *b*-value. The waveforms were compensated for concomitant gradient effects (37-39). The following imaging parameters were used: TR =9,370 ms, TE =120 ms, resolution =4.3×4.3×5.0 mm$^3$, and acquisition time =8 min 55 s. Motion and eddy-current corrections were not performed. Detailed information on the tensor-valued diffusion sequence is available at https://github.com/filip-szczepankiewicz/fwf_seq_resources.

### *Image processing and analysis*

We performed QTI analysis as described by Westin *et al.* (26). We also used the QTI parameters in a previous study by Szczepankiewicz *et al.* (25): MD, $MK_A$, $MK_I$, $MK_T$, FA, and μFA. The QTI parameters were estimated using an open-source toolbox for multidimensional diffusion MRI (40,41).

QTI analysis was performed using MATLAB (R2021b, The Mathworks, Massachusetts, USA). The regions of interest (ROIs) of the tumor were drawn using the free-hand technique on the S0 maps calculated by QTI parameters, referring to the imaging findings on the DCE images to confirm the margin of the tumor. A faculty breast radiologist with 9 years of experience drew all ROIs on each S0 map of the pre- and post-NAC MRI, excluding the areas of peritumoral edema and intratumoral necrosis. We measured the tumor size was with the greatest dimension of the tumors using a digital caliper on the DCE T1-weighted images of both pre-NAC and post-NAC MRIs.

### *Post hoc analysis*

After the previously noted faculty breast radiologist completed the measurements using QTI analyses, a faculty neuroradiologist with 14 years of experience performed a qualitative post hoc review of the images to identify potential artifacts consistently appearing on breast MRI or potential differences in the segmentation-related coding of the tumor between QTI parametric maps and conventional sequences breast MRI, particularly, DWI and DCE images.

### *Histopathologic analysis*

A faculty breast pathologist with 10 years of experience retrospectively reviewed the results of the immunohistochemical analysis of core needle biopsy and surgical specimens. The pathologic reports of core needle biopsy before NAC were used to evaluate the histologic grade according to the Nottingham modification of the Scarff-Bloom-Richardson Grading System and hormonal receptor status: estrogen receptor (ER), progesterone receptor (PR), and human epidermal growth factor receptor type 2 (Her2) (42). In addition, the pathologic reports of surgical specimens after NAC were used to assess pathologic tumor size, histologic grade, Ki-67 expression, presence of regional lymph node metastasis, and final pathologic prognostic stage according to the 8$^{th}$ edition of the AJCC (36). We classified the patients into subgroups based on hormonal receptors (negative or positive), Her2 expression (negative or positive), Ki-67 expression (low or high), histologic grade (1, 2, or 3), and AJCC pathologic prognostic stage (0, 1, 2, 3, or 4). We determined a cutoff value of 20% classify the participants into low Ki-67 expression and high Ki-67 expression groups according to the St Gallen International Expert Consensus (43).

### *Statistical analysis*

The Kolmogorov-Smirnov test was performed to evaluated the normality of the data distribution. The paired *t*-test was used to compare the QTI parameters before and after NAC. Spearman's correlation analysis was performed to evaluate the correlation of QTI parameters with tumor size and Ki-67 expression at diagnosis or after NAC. An independent *t*-test and analysis of variance (ANOVA) test was employed to analyze the differences of QTI parameters among the subgroups divided by hormonal receptor status, Her2 expression, Ki-67 expression, and final AJCC pathologic prognostic stage. For multiple comparisons, the ANOVA test with Bonferroni correction for P values were applied. We also calculated Cohen's *d* effect sizes (ES) to determine the standardized mean differences between the subgroups (44,45). Statistical significance was set at $P<0.05$ (two-sided). All statistical analyses were performed using SPSS software (version 24.0, IBM, Armonk, NY, USA) and MedCalc (version 19.8, MedCalc Software, Mariakerke, Belgium).

## Results

### *Clinicopathologic characteristics of the patients*

*Table 1* summarizes the patients' demographics and clinical. On DCE T1-weighted images, the mean tumor size was 44.0±21.5 (range, 11–104) mm on the pre-NAC MRI and 28.6±20.0 (range, 5–73) mm on the post-NAC MRI. The time between post-NAC MRI examination and surgery was 7–25 (median, 13.5) days.

### *Changes in the QTI parameters between the pre- and post-NAC MRIs with qualitative histopathological correlation*

*Table 2* summarized the changes in the QTI parameters measured from the ROI analysis of the tumors on pre- and post-NAC MRIs. $MK_T$, $MK_A$, and μFA showed significant changes between the pre- and post-NAC MRIs (0.99±0.33 *vs.* 0.81±0.41, ES: 0.48, P=0.03; 0.73±0.27 *vs.* 0.48±0.30, ES:

**Table 1** Patients' demographics and clinical characteristics

| Variables | Total (n=23) |
|---|---|
| Age at diagnosis (years) | 51.5±9.5 |
| Histologic type | |
| Invasive ductal carcinoma | 21 |
| Tubular carcinoma | 1 |
| Ductal carcinoma *in situ* | 1 |
| Hormonal subtypes | |
| Luminal type | 10 |
| Her2-enriched type | 6 |
| Triple negative type | 7 |
| Histologic grades | |
| 1 | 5 |
| 2 | 10 |
| 3 | 8 |
| Initial tumor size on MRI (mm)[†] | |
| ≥10–20 | 1 |
| >20–30 | 8 |
| >30–40 | 3 |
| >40–50 | 3 |
| >50 | 8 |
| Presence of regional lymph node metastases at diagnosis[‡] | |
| Presence | 15 |
| Absence | 8 |
| AJCC clinical prognostic cancer stage at diagnosis | |
| Stage I | 2 |
| Stage II | 7 |
| Stage III | 9 |
| Stage IV | 5 |
| AJCC prognostic cancer stage after NAC[§] | |
| Stage 0 | 3 |
| Stage I | 6 |
| Stage II | 4 |
| Stage III | 5 |
| Stage IV | 5 |

Data were presented as mean ± standard deviation or number. [†], initial tumor size defined as longest diameter on dynamic contrast-enhanced images; [‡], metastases of axillary lymph nodes at diagnosis were confirmed by fine needle aspiration biopsy; [§], AJCC prognostic cancer stage was determined in the 18 breast cancers underwent surgery, which meant pathologic prognostic staging after NAC, and that of other 5 cancers was clinical prognostic staging, because they did not underwent surgery due to distant metastases. Her2, human epidermal growth factor receptor type 2; MRI, magnetic resonance imaging; AJCC, American Joint Committee on Cancer; NAC, neoadjuvant chemotherapy.

0.88, P<0.001; 0.68±0.11 *vs.* 0.58±0.14, ES: 0.79, P=0.003; respectively). In particular, the ES for the changes in $MK_A$ and μFA was prominent between the two MRIs, suggesting that $MK_A$ and μFA outperformed other QTI parameters in quantifying changes after NAC. An example of the QTI parameter maps obtained through image processing is shown in *Figure 2*.

*Table 3* shows the correlation between tumor size changes and QTI parameters in the pre- and post-NAC MRIs. All QTI parameters showed negative correlations with change in tumor size on both pre- and post-NAC MRIs; however, the difference was not statistically significant.

In the qualitative histopathological review, the lesions showed heterogeneous cell density variation with eccentric growth and replacement along the radiating ductal structures and lobules on the pre-NAC biopsy specimen. However, pleomorphic tumor cells with eccentric growth were replaced by prominent fibrosis after NAC (*Figure 2S-2V*).

### *Correlation of the QTI parameters on the pre- and post-NAC MRIs with prognostic factors*

*Table 4* shows the QTI parameters on the pre- and post-NAC MRIs according to the prognostic factors. Tumors with high Ki-67 expression showed significantly lower pre-NAC MD and higher pre-NAC μFA than those with low Ki-67 expression (0.98±0.09 *vs.* 1.25±0.20, ES: 1.82, P=0.002; and 0.72±0.07 *vs.* 0.57±0.10, ES: 1.74, P=0.005; respectively).

According to PR status, the negative PR group showed significantly lower $MK_T$, $MK_A$, and $MK_I$ on post-NAC MRI (0.60±0.31 *vs.* 1.03±0.40, ES: 1.20, P=0.008; 0.36±0.21 *vs.* 0.61±0.33, ES: 0.90, P=0.04; and 0.23±0.17 *vs.* 0.42±0.25, ES: 0.89, P=0.046; respectively). According to the ER and Her2 status, and AJCC pathologic prognostic staging, there were no statistically significant changes in any QTI parameters.

## Discussion

In this study, we observed the following changes in QTI parameters in patients with breast cancer treated with NAC: the mean values of $MK_T$, $MK_A$, and μFA showed a significant reduction after NAC, $MK_A$ and μFA had the large ES for the changes after NAC. Tumors with high Ki-67 expression had lower MD and higher μFA on the pre-NAC MRI, and tumors with PR negativity had lower $MK_T$, $MK_A$ and $MK_I$ on the post-NAC MRI.

**Table 2** Summary of QTI parameters changes in tumors on pre- and post-NAC MRI

| QTI parameters | MD (μm²/ms) | $MK_T$ | $MK_A$ | $MK_I$ | FA | μFA |
|---|---|---|---|---|---|---|
| Pre-NAC | 1.05±0.20 | 0.99±0.33 | 0.73±0.27 | 0.26±0.12 | 0.23±0.08 | 0.68±0.11 |
| Post-NAC | 1.08±0.30 | 0.81±0.41 | 0.48±0.30 | 0.32±0.23 | 0.27±0.12 | 0.58±0.14 |
| ES | 0.12 | 0.48 | 0.88 | 0.33 | 0.39 | 0.79 |
| P value | 0.75 | 0.03 | <0.001 | 0.25 | <0.05 | 0.003 |

Data were presented as mean ± standard deviation. P values were calculated using paired *t*-test. QTI, Q-space trajectory imaging; NAC, neoadjuvant chemotherapy; MRI, magnetic resonance imaging; MD, mean diffusivity; $MK_T$, total mean kurtosis; $MK_A$, anisotropic mean kurtosis; $MK_I$, isotropic mean kurtosis; FA, macroscopic fractional anisotropy; μFA, microscopic fractional anisotropy; ES, effect size.

Tumor response to NAC is strongly associated with the survival in the breast cancer patients (46,47). Conventional DWI with ADC using single diffusion encoding is widely used clinically. Although ADC value is an efficient biomarker for estimating tumoral cellularity, it cannot distinguish the chemotherapy-related tissue changes such as fibrosis or inflammatory cell aggregation from residual viable tumor. Therefore, diffusion tensor invariants, such as DTI and DKI, have been suggested for evaluating post-NAC tumor response and predicting pathologic response (17,18). In contrast to conventional DWI, DTI can provide additional several diffusion parameters, however, previous studies demonstrated inconsistent results of the DTI-derived parameters to distinguishing malignancy from other tissue changes (16,19-21,48,49). Also, DKI, which has concept of kurtosis and diffusional variance same as tensor-valued diffusion encoding, have failed to link the kurtosis-related parameters to the tissue microstructure (10,22,23). Furthermore, advanced diffusion models have been used to evaluate post-NAC response, including the stretched exponential model and intravoxel incoherent models (50). However, these models could not explain the microstructural changes of the tumor after NAC, although the derived parameters of advanced diffusion models were predictors of the post-NAC response. To overcome this issue, tensor-valued diffusion encoding was recently developed to provide intratumoral microstructural information in multiple organs, including the breast.

The present study applied tensor-valued diffusion encoding with QTI to investigate the microstructure of breast cancer from the perspective of NAC. We observed that $MK_T$, $MK_A$, and μFA were significantly decreased in breast cancers after NAC, which was demonstrated by the loss of directionality due to the replacement of radiating ductal structures consisting of tumors with fibrosis in response to NAC, based on histopathological correlation. The results of previous studies can also explain our findings regarding NAC: (I) the increased $MK_T$, $MK_A$, and μFA values in invasive ductal carcinomas before treatment indicated microscopic anisotropy as a dominant component of diffusion restriction, resulting from the tumor growth pattern extending along the ductal system (31); and (II) tumors have a characteristic pattern of fibrosis with scattered foci of tumor cells and infiltration of lymphocytes and macrophages after NAC (51-53).

There was no significant correlation between changes in tumor size and QTI parameters after NAC. During the study period, we hypothesized that pre-NAC $MK_I$ had a negative correlation with tumor size changes after NAC based on a previous study that showed a positive correlation between $MK_I$ and tumor size (31). The reason for this discrepancy between observation and estimation remains unclear; however, it might be related to the fact that tumors undergo histological changes during NAC in which malignant cells and tumors are replaced by fibrosis and cellular infiltrations of macrophages and lymphocytes (54,55). As a result, various shrink patterns of residual tumors may emerge after NAC, which may also affect changes in tumor size (52,53,56). Further study of the pre-NAC $MK_I$ with the quantitative histopathological correlation of residual tumor pattern after NAC is required to clarify the relationship between intratumoral heterogeneity and chemotherapy response and to validate our results.

The current study also found that tumors with high Ki-67 expression had a lower mean pre-NAC MD value and a higher mean pre-NAC μFA value. This finding might be explained by the high cellularity due to the high mitotic activity of tumors with high Ki-67 expression. In addition, significant changes in μFA between pre- and post-NAC MRIs were observed tumors with high Ki-67 expression. A previous study demonstrated that tumors with high

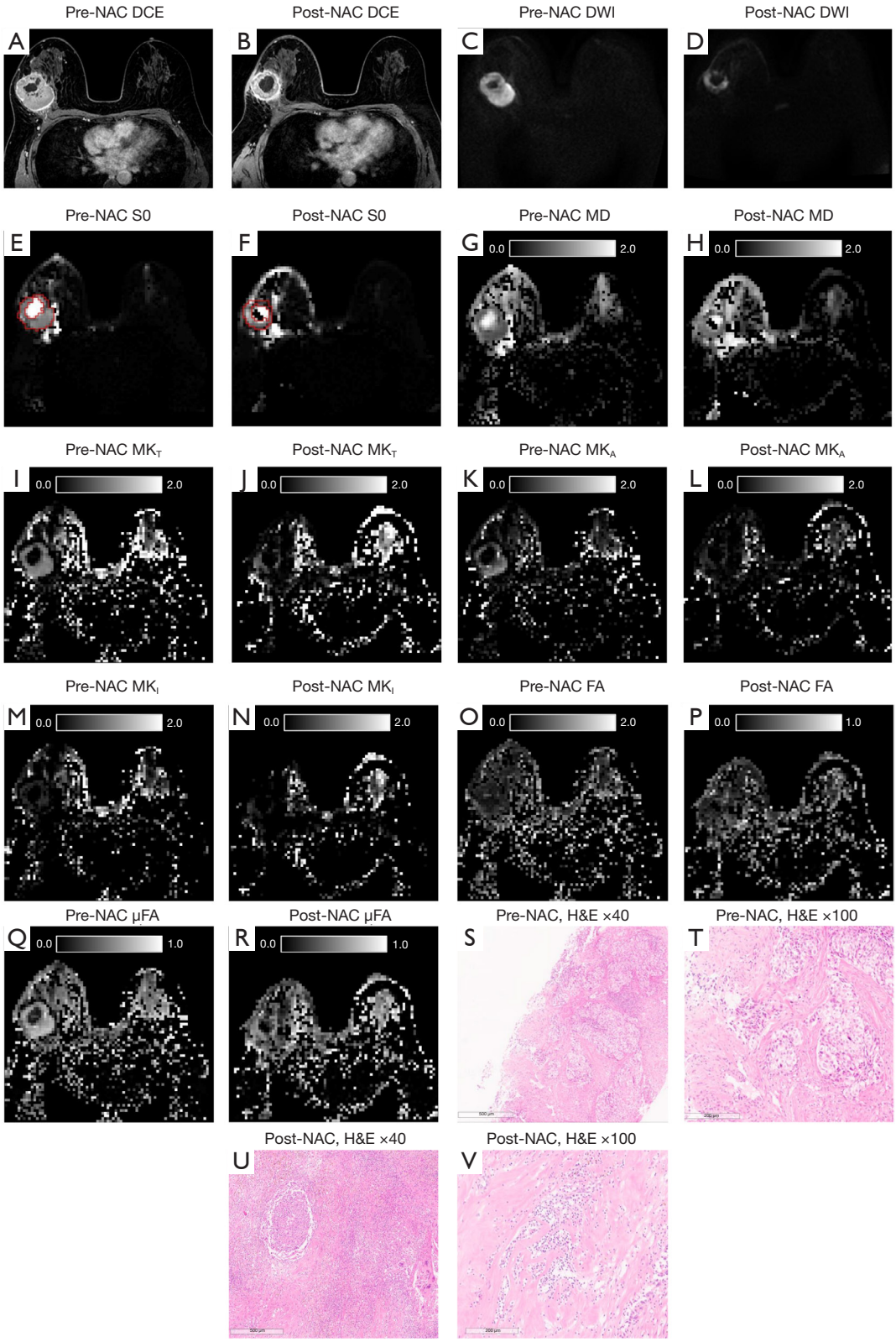


**Figure 2** A 56-year-old woman underwent NAC for the invasive ductal carcinoma in the right breast. (A) Axial DCE image of pre-NAC MRI reveals a large round shaped mass with central necrosis in the right breast at the 10 o'clock position. (B) Axial DCE image of post-

NAC MRI shows that size of the index mass is decreased after chemotherapy. (C,D) Single diffusion encoding images (*b*-value 1,500 s/mm$^2$) of pre-NAC (C) and post-NAC (D) show the prominent diffusion restriction of the tumor except central necrotic component. (E,F) Region-of-interests of the tumor are defined on S0 maps of the both pre-NAC and post-NAC MRI, referring to the DCE images and single diffusion encoding image. (G,H) MD becomes slightly increased between the pre-NAC (G, mean MD, 0.91 μm$^2$/ms) and the post-NAC (H, mean MD, 1.24 μm$^2$/ms) MRI. (I,J) $MK_T$ of the tumor decreases between the pre-NAC (I) and the post-NAC (J) MRI. (K-N) Between the pre- and post-NAC $MK_A$ (K,L) and $MK_I$ (M,N) maps, the tumor exhibits a decrease in $MK_A$. (O,P) FA map reveals insignificant changes of FA in the tumor between the pre-NAC (O) and post-NAC (P) MRI. (Q,R) Compared to the pre-NAC map, μFA decreases on the post-NAC map. (S,T) Histopathological examination of a specimen from the core needle biopsy at the time of diagnosis reveals that tumor cluster composed of pleomorphic tumor cells with sheet-like growth pattern. (U,V) Histopathological examination of a specimen from the breast conserving surgery after NAC shows that between the area of residual tumor cluster is loose connective tissue with giant cell aggregation and hemosiderin-laden pigments [×40 magnification (S and U); ×100 magnification (T and V); H&E]. NAC, neoadjuvant chemotherapy; DCE, dynamic contrast-enhanced; DWI, diffusion-weighted imaging; MD, mean diffusivity; $MK_T$, total mean kurtosis; $MK_A$, anisotropic mean kurtosis; $MK_I$, isotropic mean kurtosis; FA, fractional anisotropy; μFA, microscopic fractional anisotropy; H&E, hematoxylin and eosin stain; MRI, magnetic resonance imaging.

**Table 3** Correlation between tumor size changes on MRI and QTI parameters on pre- and post-NAC MRI

| Tumor size changes | MD (μm$^2$/ms) | $MK_T$ | $MK_A$ | $MK_I$ | FA | μFA |
|---|---|---|---|---|---|---|
| Pre-NAC | | | | | | |
| $r_s$ | −0.07 | −0.21 | −0.12 | −0.33 | −0.30 | 0.06 |
| P value | 0.74 | 0.33 | 0.60 | 0.12 | 0.17 | 0.80 |
| Post-NAC | | | | | | |
| $r_s$ | 0.20 | 0.03 | −0.18 | 0.16 | −0.12 | −0.09 |
| P value | 0.36 | 0.89 | 0.40 | 0.48 | 0.59 | 0.67 |

$r_s$, Spearman's rank correlation coefficient; P values were calculated using Spearman's correlation analysis. MRI, magnetic resonance imaging; QTI, Q-space trajectory imaging; NAC, neoadjuvant chemotherapy; MD, mean diffusivity; $MK_T$, total mean kurtosis; $MK_A$, anisotropic mean kurtosis; $MK_I$, isotropic mean kurtosis; FA, macroscopic fractional anisotropy; μFA, microscopic fractional anisotropy.

Ki-67 expression, which indicate high cellularity due to increased proliferation and the presence of abundant radiating structures, are associated with a favorable clinical response to NAC (57,58). In addition, $MK_A$ and μFA are closely related parameters that reflect the diffusional anisotropy due to the eccentric and radiating characteristics of the tumor (25). Therefore, our findings suggest that the loss of diffusional anisotropy as a replacement for the microstructures occurred in response to NAC.

We also evaluated the correlation between hormone receptor status and QTI parameters on pre- and post-NAC MRIs. Interestingly, the PR negative group showed significantly lower $MK_T$, $MK_A$, and $MK_I$ values on post-NAC MRI than on pre-NAC MRI. Considering the results of previous studies that demonstrated the negativity of PR status as independent predictor of pathologic complete remission (59,60), our findings suggest that tumors with a negative PR status might be associated with a better response to NAC. In contrast, the ER and Her2 status, and AJCC pathologic prognostic staging did not show statistically significant changes in any QTI parameter related to NAC. Considering these findings, we consider the following factor as a possible explanation: according to the 8$^{th}$ edition of the AJCC, even for tumors with similar size, nodal metastasis, and proliferative index, the prognostic stage varies depending on the hormonal subtype; therefore, microstructural changes in tumors might not directly affect to the AJCC staging.

This study has some limitations that should be considered. First, this was a retrospective preliminary study with a relatively small and heterogeneous cohort of patients from a single institution, introducing potential selection bias and limiting the subgroup analyses for molecular subtype and cancer staging. Second, the in-plane resolution of tensor-valued diffusion encoding was low, which may have affected the delineation of tumors due to partial volume

**Table 4** QTI parameters on pre- and post-NAC MRI according to the prognostic factors

| Prognostic factors | Items | No. | MD ($\mu m^2$/ms) | | $MK_T$ | | $MK_A$ | | $MK_I$ | | FA | | μFA | |
|---|---|---|---|---|---|---|---|---|---|---|---|---|---|---|
| | | | Pre- | Post- | Pre- | Post- | Pre- | Post- | Pre- | Post- | Pre- | Post- | Pre- | Post- |
| Estrogen receptor | Positive | 12 | 1.06±0.23 | 1.10±0.34 | 1.05±0.39 | 0.88±0.50 | 0.79±0.32 | 0.54±0.37 | 0.26±0.10 | 0.34±0.26 | 0.22±0.07 | 0.28±0.14 | 0.66±0.13 | 0.60±0.15 |
| | Negative | 11 | 1.04±0.17 | 1.05±0.26 | 0.93±0.24 | 0.73±0.28 | 0.67±0.21 | 0.42±0.18 | 0.27±0.13 | 0.30±0.20 | 0.23±0.10 | 0.27±0.11 | 0.70±0.08 | 0.56±0.12 |
| | P value | | 0.80 | 0.71 | 0.45 | 0.39 | 0.29 | 0.35 | 0.73 | 0.69 | 0.80 | 0.88 | 0.44 | 0.74 |
| | ES | | 0.10 | 0.17 | 0.37 | 0.37 | 0.44 | 0.41 | 0.09 | 0.17 | 0.12 | 0.08 | 0.37 | 0.29 |
| Progesterone receptor | Positive | 11 | 1.00±0.18 | 1.03±0.31 | 1.12±0.32 | 1.03±0.40 | 0.84±0.27 | 0.61±0.33 | 0.28±0.10 | 0.42±0.25 | 0.23±0.07 | 0.28±0.15 | 0.69±0.10 | 0.61±0.15 |
| | Negative | 12 | 1.11±0.22 | 1.11±0.30 | 0.88±0.30 | 0.60±0.31 | 0.63±0.24 | 0.36±0.21 | 0.25±0.13 | 0.23±0.17 | 0.23±0.10 | 0.27±0.11 | 0.67±0.12 | 0.56±0.12 |
| | P value | | 0.20 | 0.54 | 0.08 | 0.008 | 0.06 | 0.04 | 0.58 | 0.046 | 0.99 | 0.97 | 0.59 | 0.31 |
| | ES | | 0.55 | 0.26 | 0.77 | 1.20 | 0.82 | 0.90 | 0.26 | 0.89 | 0.00 | 0.08 | 0.26 | 0.37 |
| Human epidermal growth factor receptor type 2 | Positive | 6 | 1.14±0.19 | 1.27±0.29 | 0.95±0.24 | 0.57±0.50 | 0.64±0.19 | 0.36±0.34 | 0.31±0.10 | 0.22±0.17 | 0.21±0.06 | 0.22±0.11 | 0.67±0.08 | 0.52±0.12 |
| | Negative | 17 | 1.02±0.20 | 1.01±0.28 | 1.01±0.36 | 0.89±0.36 | 0.76±0.29 | 0.53±0.28 | 0.25±0.12 | 0.36±0.24 | 0.23±0.09 | 0.29±0.12 | 0.68±0.12 | 0.60±0.14 |
| | P value | | 0.25 | 0.058 | 0.72 | 0.11 | 0.36 | 0.24 | 0.26 | 0.18 | 0.55 | 0.20 | 0.76 | 0.21 |
| | ES | | 0.62 | 0.91 | 0.20 | 0.73 | 0.49 | 0.55 | 0.54 | 0.67 | 0.26 | 0.61 | 0.10 | 0.61 |
| Ki-67 index[†] | <20% | 5 | 1.25±0.20 | 0.96±0.34 | 0.92±0.56 | 0.81±0.62 | 0.69±0.46 | 0.41±0.37 | 0.24±0.10 | 0.41±0.33 | 0.21±0.04 | 0.27±0.04 | 0.57±0.10 | 0.57±0.14 |
| | ≥20% | 12 | 0.98±0.09 | 1.05±0.26 | 1.03±0.23 | 0.88±0.35 | 0.76±0.20 | 0.52±0.27 | 0.27±0.13 | 0.36±0.23 | 0.22±0.09 | 0.31±0.13 | 0.72±0.07 | 0.60±0.14 |
| | P value | | 0.002 | 0.58 | 0.57 | 0.79 | 0.63 | 0.51 | 0.63 | 0.73 | 0.75 | 0.52 | 0.005 | 0.76 |
| | ES | | 1.82 | 0.30 | 0.26 | 0.14 | 0.20 | 0.34 | 0.26 | 0.18 | 0.14 | 0.42 | 1.74 | 0.21 |
| AJCC prognostic stages after NAC[‡] | Stage 0 | 3 | 1.02±0.10 | 1.14±0.44 | 0.94±0.17 | 0.69±0.52 | 0.65±0.13 | 0.33±0.22 | 0.29±0.05 | 0.35±0.31 | 0.20±0.05 | 0.28±0.10 | 0.68±0.03 | 0.59±0.03 |
| | Stage I | 6 | 1.14±0.09 | 0.96±0.38 | 1.04±0.34 | 0.83±0.55 | 0.78±0.30 | 0.44±0.39 | 0.26±0.08 | 0.38±0.33 | 0.22±0.10 | 0.33±0.16 | 0.66±0.07 | 0.57±0.18 |
| | Stage II | 4 | 0.99±0.05 | 1.01±0.31 | 0.73±0.31 | 0.77±0.29 | 0.60±0.28 | 0.43±0.21 | 0.14±0.04 | 0.34±0.29 | 0.25±0.13 | 0.29±0.17 | 0.64±0.13 | 0.53±0.10 |
| | Stage III | 5 | 1.19±0.32 | 1.31±0.13 | 0.90±0.38 | 0.68±0.31 | 0.67±0.31 | 0.42±0.18 | 0.26±0.14 | 0.26±0.13 | 0.18±0.05 | 0.19±0.06 | 0.65±0.16 | 0.53±0.11 |
| | Stage IV | 5 | 0.89±0.17 | 0.99±0.15 | 1.26±0.20 | 1.01±0.43 | 0.90±0.25 | 0.72±0.32 | 0.36±0.11 | 0.28±0.12 | 0.27±0.07 | 0.28±0.10 | 0.77±0.06 | 0.69±0.14 |
| | P value | | 0.12 | 0.34 | 0.17 | 0.78 | 0.48 | 0.35 | 0.054 | 0.92 | 0.56 | 0.53 | 0.29 | 0.33 |
| | ES | | 1.50 | 1.17 | 1.61 | 0.81 | 1.11 | 1.30 | 1.83 | 0.52 | 1.13 | 1.17 | 1.18 | 1.14 |

Data were presented as mean ± standard deviation. [†], Ki-67 index was measured only in the 17 patients; [‡], AJCC prognostic cancer stage was determined in the 18 breast cancers underwent surgery, which meant pathologic prognostic staging after NAC, and that of other 5 cancers was clinical prognostic staging, because they did not underwent surgery due to distant metastases. P values for tests for equal mean values from independent *t*-test or analysis of variance test. QTI, Q-space trajectory imaging; NAC, neoadjuvant chemotherapy; MRI, magnetic resonance imaging; MD, mean diffusivity; $MK_T$, total mean kurtosis; $MK_A$, anisotropic mean kurtosis; $MK_I$, isotropic mean kurtosis; FA, macroscopic fractional anisotropy; μFA, microscopic fractional anisotropy; ES, effect size; AJCC, American Joint Committee on Cancer.

effects. This issue could be mitigated by increasing the acquisition time; however, this can reduce clinical feasibility due to the scan time exceeding 13 minutes. Third, motion correction was not applied to the prototype sequence. Implementing the correction method is expected to improve the spatial sharpness and accuracy of the parameter estimation. Lastly, the QTI parameters in our study were analyzed with qualitative radiologic-pathologic correlation for the core needle biopsy and surgical specimens, whereas the previous study employed quantitative microscopy (25). Further studies analyzing QTI parameters in breast cancer that are correlated with quantitative histopathology are needed to validate our results.

## Conclusions

We found that the QTI parameters reflected microstructural changes in breast cancer after NAC. The significant post-NAC changes in $MK_T$, $MK_A$, and μFA indicate a reduction in radiating microstructures and replacement with fibrotic stroma in breast cancers. Of the three parameters, $MK_A$ and μFA were superior in evaluating post-NAC tumor changes, which reflected diffusional anisotropic component. In addition, QTI parameters were correlated with prognostic factors, such as Ki-67 expression and PR status. Therefore, QTI parameters derived from tensor-valued diffusion encoding can serve as non-invasive imaging biomarkers for assessing the post-NAC response of breast cancers by providing intratumoral microstructural information.

## Acknowledgments

*Funding:* None.

## Footnote

*Reporting Checklist:* The authors have completed the STROBE reporting checklist. Available at https://gs.amegroups.com/article/view/10.21037/gs-24-124/rc

*Data Sharing Statement:* Available at https://gs.amegroups.com/article/view/10.21037/gs-24-124/dss

*Peer Review File:* Available at https://gs.amegroups.com/article/view/10.21037/gs-24-124/prf

*Conflicts of Interest:* All authors have completed the ICMJE uniform disclosure form (available at https://gs.amegroups.com/article/view/10.21037/gs-24-124/coif). F.S. is co-inventor in technology related to this research and has financial interests in Random Walk Imaging AB. The other authors have no conflicts of interest to declare.

*Ethical Statement:* The authors are accountable for all aspects of the work in ensuring that questions related to the accuracy or integrity of any part of the work are appropriately investigated and resolved. This study was conducted according to the Declaration of Helsinki (as revised in 2013). Approval was granted by the Institutional Review Board of Gyeongsang National University Changwon Hospital (IRB No. GNUCH 2023-03-043). Patients' informed consent to participate was waived in view of the retrospective nature of the study.



## References

1. Goldhirsch A, Glick JH, Gelber RD, et al. Meeting highlights: International Consensus Panel on the Treatment of Primary Breast Cancer. Seventh International Conference on Adjuvant Therapy of Primary Breast Cancer. J Clin Oncol 2001;19:3817-27.
2. Mougalian SS, Soulos PR, Killelea BK, et al. Use of neoadjuvant chemotherapy for patients with stage I to III breast cancer in the United States. Cancer 2015;121:2544-52.
3. Croshaw R, Shapiro-Wright H, Svensson E, et al. Accuracy of clinical examination, digital mammogram, ultrasound, and MRI in determining postneoadjuvant pathologic tumor response in operable breast cancer patients. Ann Surg Oncol 2011;18:3160-3.
4. Scheel JR, Kim E, Partridge SC, et al. MRI, Clinical Examination, and Mammography for Preoperative Assessment of Residual Disease and Pathologic Complete Response After Neoadjuvant Chemotherapy for Breast Cancer: ACRIN 6657 Trial. AJR Am J Roentgenol 2018;210:1376-85.

5. Baltzer P, Mann RM, Iima M, et al. Diffusion-weighted imaging of the breast-a consensus and mission statement from the EUSOBI International Breast Diffusion-Weighted Imaging working group. Eur Radiol 2020;30:1436-50.
6. Gullo RL, Partridge SC, Shin HJ, et al. Update on DWI for Breast Cancer Diagnosis and Treatment Monitoring. AJR Am J Roentgenol 2024;222:e2329933.
7. Le Bihan D, Breton E, Lallemand D, et al. MR imaging of intravoxel incoherent motions: application to diffusion and perfusion in neurologic disorders. Radiology 1986;161:401-7.
8. Sharma U, Danishad KK, Seenu V, et al. Longitudinal study of the assessment by MRI and diffusion-weighted imaging of tumor response in patients with locally advanced breast cancer undergoing neoadjuvant chemotherapy. NMR Biomed 2009;22:104-13.
9. Nilsen L, Fangberget A, Geier O, et al. Diffusion-weighted magnetic resonance imaging for pretreatment prediction and monitoring of treatment response of patients with locally advanced breast cancer undergoing neoadjuvant chemotherapy. Acta Oncol 2010;49:354-60.
10. Zhuang Z, Zhang Q, Zhang D, et al. Utility of apparent diffusion coefficient as an imaging biomarker for assessing the proliferative potential of invasive ductal breast cancer. Clin Radiol 2018;73:473-8.
11. Woodhams R, Kakita S, Hata H, et al. Identification of residual breast carcinoma following neoadjuvant chemotherapy: diffusion-weighted imaging--comparison with contrast-enhanced MR imaging and pathologic findings. Radiology 2010;254:357-66.
12. Bufi E, Belli P, Costantini M, et al. Role of the Apparent Diffusion Coefficient in the Prediction of Response to Neoadjuvant Chemotherapy in Patients With Locally Advanced Breast Cancer. Clin Breast Cancer 2015;15:370-80.
13. Marini C, Iacconi C, Giannelli M, et al. Quantitative diffusion-weighted MR imaging in the differential diagnosis of breast lesion. Eur Radiol 2007;17:2646-55.
14. Woodhams R, Matsunaga K, Kan S, et al. ADC mapping of benign and malignant breast tumors. Magn Reson Med Sci 2005;4:35-42.
15. Hahn SY, Ko EY, Han BK, et al. Role of diffusion-weighted imaging as an adjunct to contrast-enhanced breast MRI in evaluating residual breast cancer following neoadjuvant chemotherapy. Eur J Radiol 2014;83:283-8.
16. Wilmes LJ, Li W, Shin HJ, et al. Diffusion Tensor Imaging for Assessment of Response to Neoadjuvant Chemotherapy in Patients With Breast Cancer. Tomography 2016;2:438-47.
17. Zhang D, Geng X, Suo S, et al. The predictive value of DKI in breast cancer: Does tumour subtype affect pathological response evaluations? Magn Reson Imaging 2022;85:28-34.
18. Furman-Haran E, Nissan N, Ricart-Selma V, et al. Quantitative evaluation of breast cancer response to neoadjuvant chemotherapy by diffusion tensor imaging: Initial results. J Magn Reson Imaging 2018;47:1080-90.
19. Furman-Haran E, Grobgeld D, Nissan N, et al. Can diffusion tensor anisotropy indices assist in breast cancer detection? J Magn Reson Imaging 2016;44:1624-32.
20. Cakir O, Arslan A, Inan N, et al. Comparison of the diagnostic performances of diffusion parameters in diffusion weighted imaging and diffusion tensor imaging of breast lesions. Eur J Radiol 2013;82:e801-6.
21. Partridge SC, Ziadloo A, Murthy R, et al. Diffusion tensor MRI: preliminary anisotropy measures and mapping of breast tumors. J Magn Reson Imaging 2010;31:339-47.
22. Tietze A, Hansen MB, Østergaard L, et al. Mean Diffusional Kurtosis in Patients with Glioma: Initial Results with a Fast Imaging Method in a Clinical Setting. AJNR Am J Neuroradiol 2015;36:1472-8.
23. Le Bihan D. Apparent diffusion coefficient and beyond: what diffusion MR imaging can tell us about tissue structure. Radiology 2013;268:318-22.
24. Afzali M, Mueller L, Szczepankiewicz F, et al. Quantification of Tissue Microstructure Using Tensor-Valued Diffusion Encoding: Brain and Body. Front Phys 2022;10:809133.
25. Szczepankiewicz F, van Westen D, Englund E, et al. The link between diffusion MRI and tumor heterogeneity: Mapping cell eccentricity and density by diffusional variance decomposition (DIVIDE). Neuroimage 2016;142:522-32.
26. Westin CF, Knutsson H, Pasternak O, et al. Q-space trajectory imaging for multidimensional diffusion MRI of the human brain. Neuroimage 2016;135:345-62.
27. Nery F, Szczepankiewicz F, Kerkelä L, et al. In vivo demonstration of microscopic anisotropy in the human kidney using multidimensional diffusion MRI. Magn Reson Med 2019;82:2160-8.
28. Langbein BJ, Szczepankiewicz F, Westin CF, et al. A Pilot Study of Multidimensional Diffusion MRI for Assessment of Tissue Heterogeneity in Prostate Cancer. Invest Radiol 2021;56:845-53.
29. Naranjo ID, Reymbaut A, Brynolfsson P, et al.


 

Multidimensional Diffusion Magnetic Resonance Imaging for Characterization of Tissue Microstructure in Breast Cancer Patients: A Prospective Pilot Study. Cancers (Basel) 2021;13:1606.
30. Brabec J, Szczepankiewicz F, Lennartsson F, et al. Histogram analysis of tensor-valued diffusion MRI in meningiomas: Relation to consistency, histological grade and type. Neuroimage Clin 2022;33:102912.
31. Cho E, Baek HJ, Szczepankiewicz F, et al. Clinical experience of tensor-valued diffusion encoding for microstructure imaging by diffusional variance decomposition in patients with breast cancer. Quant Imaging Med Surg 2022;12:2002-17.
32. Teh I, Shelley D, Boyle JH, et al. Cardiac q-space trajectory imaging by motion-compensated tensor-valued diffusion encoding in human heart in vivo. Magn Reson Med 2023;90:150-65.
33. Cory D, Garroway A, Miller J. Applications of spin transport as a probe of local geometry. Abstracts of Papers of the American Chemical Society. Washington, USA; 1990.
34. Callaghan PT. Translational Dynamics and Magnetic Resonance: Principles of Pulsed Gradient Spin Echo NMR. Oxford: Oxford Academic; 2011.
35. Lasič S, Szczepankiewicz F, Eriksson S, et al. Microanisotropy imaging: quantification of microscopic diffusion anisotropy and orientational order parameter by diffusion MRI with magic-angle spinning of the q-vector. Front Phys 2014;2:11.
36. Amin MB, Edge SB, Greene FL, et al. AJCC Cancer Staging Manual, 8th ed. New York: Springer; 2017.
37. Sjölund J, Szczepankiewicz F, Nilsson M, et al. Constrained optimization of gradient waveforms for generalized diffusion encoding. J Magn Reson 2015;261:157-68.
38. Szczepankiewicz F, Westin CF, Nilsson M. Maxwell-compensated design of asymmetric gradient waveforms for tensor-valued diffusion encoding. Magn Reson Med 2019;82:1424-37.
39. Szczepankiewicz F, Westin CF, Nilsson M. Gradient waveform design for tensor-valued encoding in diffusion MRI. J Neurosci Methods 2021;348:109007.
40. Available online: https://github.com/markus-nilsson/md-dmri. Accessed April 04, 2024.
41. Nilsson M, Szczepankiewicz F, Lampinen B, et al. An open-source framework for analysis of multidimensional diffusion MRI data implemented in MATLAB. In: Proc Intl Soc Mag Reson Med; Paris, France; 2018.
42. Elston CW, Ellis IO. Pathological prognostic factors in breast cancer. I. The value of histological grade in breast cancer: experience from a large study with long-term follow-up. Histopathology 1991;19:403-10.
43. Goldhirsch A, Winer EP, Coates AS, et al. Personalizing the treatment of women with early breast cancer: highlights of the St Gallen International Expert Consensus on the Primary Therapy of Early Breast Cancer 2013. Ann Oncol 2013;24:2206-23.
44. Cohen J. Statistical power analysis for the behavioral sciences, 2nd ed. New York: Lawrence Erlbaum Associates; 1988.
45. Olejnik S, Algina J. Measures of Effect Size for Comparative Studies: Applications, Interpretations, and Limitations. Contemp Educ Psychol 2000;25:241-86.
46. Symmans WF, Peintinger F, Hatzis C, et al. Measurement of residual breast cancer burden to predict survival after neoadjuvant chemotherapy. J Clin Oncol 2007;25:4414-22.
47. Romero A, García-Sáenz JA, Fuentes-Ferrer M, et al. Correlation between response to neoadjuvant chemotherapy and survival in locally advanced breast cancer patients. Ann Oncol 2013;24:655-61.
48. Eyal E, Shapiro-Feinberg M, Furman-Haran E, et al. Parametric diffusion tensor imaging of the breast. Invest Radiol 2012;47:284-91.
49. Baltzer PA, Schäfer A, Dietzel M, et al. Diffusion tensor magnetic resonance imaging of the breast: a pilot study. Eur Radiol 2011;21:1-10.
50. Almutlaq ZM, Wilson DJ, Bacon SE, et al. Evaluation of Monoexponential, Stretched-Exponential and Intravoxel Incoherent Motion MRI Diffusion Models in Early Response Monitoring to Neoadjuvant Chemotherapy in Patients With Breast Cancer-A Preliminary Study. J Magn Reson Imaging 2022;56:1079-88.
51. Sahoo S, Lester SC. Pathology of breast carcinomas after neoadjuvant chemotherapy: an overview with recommendations on specimen processing and reporting. Arch Pathol Lab Med 2009;133:633-42.
52. Ko ES, Han BK, Kim RB, et al. Analysis of factors that influence the accuracy of magnetic resonance imaging for predicting response after neoadjuvant chemotherapy in locally advanced breast cancer. Ann Surg Oncol 2013;20:2562-8.
53. Loo CE, Straver ME, Rodenhuis S, et al. Magnetic resonance imaging response monitoring of breast cancer during neoadjuvant chemotherapy: relevance of breast cancer subtype. J Clin Oncol 2011;29:660-6.
54. Moreno A, Escobedo A, Benito E, et al. Pathologic changes related to CMF primary chemotherapy in breast

 

cancer. Pathological evaluation of response predicts clinical outcome. Breast Cancer Res Treat 2002;75:119-25.
55. Masood S. Neoadjuvant chemotherapy in breast cancers. Womens Health (Lond) 2016;12:480-91.
56. Wang S, Zhang Y, Yang X, et al. Shrink pattern of breast cancer after neoadjuvant chemotherapy and its correlation with clinical pathological factors. World J Surg Oncol 2013;11:166.
57. Fasching PA, Heusinger K, Haeberle L, et al. Ki67, chemotherapy response, and prognosis in breast cancer patients receiving neoadjuvant treatment. BMC Cancer 2011;11:486.
58. Urruticoechea A, Smith IE, Dowsett M. Proliferation marker Ki-67 in early breast cancer. J Clin Oncol 2005;23:7212-20.
59. Li XB, Krishnamurti U, Bhattarai S, et al. Biomarkers Predicting Pathologic Complete Response to Neoadjuvant Chemotherapy in Breast Cancer. Am J Clin Pathol 2016;145:871-8.
60. Boland MR, Ryan ÉJ, Nugent T, et al. Impact of progesterone receptor status on response to neoadjuvant chemotherapy in estrogen receptor-positive breast cancer patients. J Surg Oncol 2020;122:861-8.

**Cite this article as:** Cho E, Baek HJ, Szczepankiewicz F, An HJ, Jung EJ. Imaging evaluation focused on microstructural tissue changes using tensor-valued diffusion encoding in breast cancers after neoadjuvant chemotherapy: is it a promising way forward? Gland Surg 2024;13(8):1387-1399. doi: 10.21037/gs-24-124